Using kinetic isotope effect to evaluate the significance of the sequential and parallel steps: formation of microbial consortium during reversible anaerobic methane oxidation coupled with sulfate reduction

Vasily Vavilin, Lyudmila Lokshina and Sergey Rytov

ABSTRACT

The purpose of this study was to describe the dynamics of anaerobic oxidation of methane (AOM) coupled with sulfate reduction (SR) using experimental data from a continuous incubation experiments published earlier in order to show that formation of consortia of anaerobic archaea (ANME) and *Desulfosarcina*-like bacteria (DSS) may have a significant effect on sulfur isotope fractionation. The dynamic simulation of reversible AOM by ANME coupled with SR by DSS was performed. This simulation took into account biomass growth and fractionation of stable isotopes of sulfur. Two kinetic schemes with and without ANME + DSS consortium formation were tested. The respective models were applied at five influent methane concentrations. A good fit to experimental data was obtained only when assuming active ANME and DSS biomass accumulation. The assumption about incorporation of reversibility of anaerobic methane oxidation and sulfate reduction did not improve the model's fit to experimental data. In accordance with both the models, sulfur isotope fractionation was smallest for the highest influent methane concentration. The model considering the formation of consortia of ANME + DSS is proved to be more appropriate.

Key words | anaerobic methane oxidation with sulfate, consortium of ANME + DSS, dynamic models, stoichiometry, sulfur isotope fractionation

Vasily Vavilin (corresponding author)
Lyudmila Lokshina
Sergey Rytov
Water Problems Institute,
Russian Academy of Sciences,
3 Gubkina str., Moscow 119333,
Russian Federation
E-mail: *vavilin@iwp.ru*

INTRODUCTION

In marine sediments, anaerobic oxidation of methane (AOM) accounts for 80 to 85% of total marine methane oxidation (Hinrich & Boetius 2002), substantially limiting the release of methane to the atmosphere. During AOM, methane is oxidized with sulfate as the terminal electron acceptor. This process is mediated by a syntrophic consortium of anaerobic archaea (ANME) and *Desulfosarcina*-like bacteria (DSS), which often form small aggregates (Boetius *et al.* 2000; Knittel & Boetius 2009) or voluminous mats with the net reaction:

$$CH_4 + SO_4^{2-} \rightarrow HCO_3^- + HS^- + H_2O \ (\Delta G^0 = -16.6\ \mathrm{kJ\ mol^{-1}}) \quad (1)$$

doi: 10.2166/wst.2019.201

Most of the diversity of sulfate-reducing bacteria (SRB) in hydrate-bearing sediments comprises seep-endemic clades (Knittel *et al.* 2003). Using fluorescence *in situ* hybridization on samples from six different AOM sites, SEEP-SRB1a was identified as a sulfate-reducing partner in up to 95% of total ANME-2 consortia (Schreiber *et al.* 2010). According to Beal *et al.* (2011), it has not been well recognized how the relationship between the rates of AOM and sulfate reduction (SR) varies with sulfate concentrations.

The net reaction operates near thermodynamic equilibrium (Thauer 2011). The reversible character of enzymatic reactions during AOM may decrease the rate of the net reaction (Holler *et al.* 2011) down to 5–10% of the total reaction rate. Batch enrichment cultures originating from sediments with high AOM activity and without background methanogenesis from detrital remnants were studied by Holler *et al.* (2009) to determine carbon and hydrogen isotopic

fractionation factors. The enrichment cultures, which had originated from three marine habitats (Hydrate Ridge, NE Pacific; Amon Mud Volcano, Mediterranean Sea; NW shelf, Black Sea), were dominated by archaeal phylotypes of anaerobic methanotrophs (ANME-2). Using the traditional Rayleigh's approach, Holler *et al.* (2009) concluded that there was no satisfying explanation for the variation of the fractionation factors between the cultures of different origin.

Methanol, hydrogen, methanethiol, acetate, and carbon monoxide were excluded from being involved in AOM (review article by Timmers *et al.* (2017)). Milucka *et al.* (2012) showed that zero-valent sulfur compounds (S^0) are formed during AOM through a new pathway of dissimilatory sulfate reduction performed by ANME alone. By studying sulfur isotope effects caused by AOM-SR under continuous incubation at various methane influent concentrations, Deusner *et al.* (2014) showed that the smallest sulfur and oxygen isotope fractionation was observed for the highest influent methane concentration with the highest AOM-SR rate. This phenomenon apparently contradicts the general conclusion that the rates of concentration changes of heavier substrates, products and biomasses usually are proportional to the rates of concentration changes of the total (light + heavier) substrates, products and biomasses, respectively (Vavilin *et al.* 2017, 2018a, 2018b).

The purpose of this study was to describe the dynamics of AOM-SR using Deusner's experimental data in order to show that formation of consortia of ANME + DSS may have a significant effect on sulfur isotope fractionation.

MATERIAL AND METHODS

Description of Deusner's experiments

The detailed experimental procedure was described in Deusner *et al.* (2014). In brief, in the AOM-SR experiments conducted at different influent methane concentrations, a two-stage high-pressure continuous incubation experimental system was used. The two-stage system consisted of pressurized vessels for gas enrichment and biomass incubation. The total time of incubation was 129 days. During that time, the influent concentration of dissolved methane was stepwise increased from 1.4 to 58.8 mM (1.4 ± 0.6, 2.3 ± 0.5, 6.4 ± 0.5, 11.2 ± 1.2, 22.1 ± 1.6, 43.2 ± 2.5, and 58.8 ± 10.5 mM). Data obtained for the five influent methane concentrations excluding the first (data too noisy) and the last (not enough measurements of isotope signatures) concentrations were used in our modelling.

In those experiments, the biomass originated from homogenized microbial mats of the Black Sea. Its initial dry-weight concentration in the reactor was about 4.6 $g_{DW}\,L^{-1}$. The dilution rate of the reactor volume was 1.7 d^{-1}. The anoxic medium was delivered at a constant rate with a high-pressure pump into a gas-saturation vessel pressurized with methane. The influent entered the pressurized reactor near its bottom while the effluent was coming out from the upper part of the reactor. Because of a strong tendency for biomass aggregation and sedimentation, it was presumed that the biomass was almost completely retained within the incubation vessel during long-term incubation.

Dynamic model

To create the dynamic model of AOM-SR we followed five major steps outlined below:

(i) wrote stoichiometric reactions of AOM and SR that included mass balance of sulfur and biomasses of ANME and DSS;
(ii) added dynamic equations describing the rates of biomass growth and substrate consumption;
(iii) combined equations created in the first two steps into a general model of the continuous-flow reactor carrying out reversible AOM-SR;
(iv) modified equations created in step (iii) to describe changes in sulfur stable isotope ratios during AOM-SR;
(v) wrote a dynamic equation describing formation of ANME + DSS consortium in the process of AOM-SR.

Stoichiometry

The following stoichiometric reactions that include sulfur-containing cell biomass can be written for AOM and SR with zero-valent sulfur HS_2^- as an intermediate product:

$$\begin{aligned} &7CH_4 + (8 - (20 - x)\,Y_{ANME})\,SO_4^{2-} + 7Y_{ANME}NH_4^+ \\ &\quad = 7Y_{ANME}C_5H_7NO_2S_x + \\ &(4 - (10 + 3x)\,Y_{ANME})\,HS_2^- + (7 - 35Y_{ANME})HCO_3^- \\ &\quad + (6 + (13 - x)\,Y_{ANME})\,H_2O + \\ &(5 - (2 - 5x)\,Y_{ANME})\,OH^- \end{aligned} \tag{2}$$

$$\begin{aligned} &(4 + (10 + 3z)\,Y_{DSS})\,HS_2^- + (4 - (11 + 4z)\,Y_{DSS})\,H_2O \\ &\quad + 35\,Y_{DSS}HCO_3^- + 7Y_{DSS}NH_4^+ = \\ &7Y_{DSS}C_5H_7NO_2S_z + (1 + (20 - z)\,Y_{DSS})\,SO_4^{2-} + 7\,HS^- \\ &\quad + (5 + (2 - 5z)\,Y_{DSS})\,H^+ \end{aligned} \tag{3}$$

where Y_{ANME} and Y_{DSS} are the biomass yield coefficients for ANME and DSS, respectively; x and z are the fractions of the sulfur element in microbial cells of ANME and DSS, respectively. In the model, the values of $x = 0.15$ and $z = 0.3$ were used based on the measurements of Fagerbakke *et al.* (1996) who estimated the mean S:C ratio for bacterial aquatic species to be 0.031, with a range of 0.016–0.084 and a lower value more typical for ANME than for DSS. Recently, He *et al.* (2019) presented a model of microbial interactions in the AOM combining reaction kinetics and energetics, but a biomass growth in archaeal-bacterial consortia was not considered.

It should be emphasized that the mechanism of AOM-SR still remains unclear (Timmers *et al.* 2017), and the formation of intermediate disulfide is our assumption based on the articles by Milucka *et al.* (2012), Deusner *et al.* (2014), McGlynn (2017), and He *et al.* (2019). In accordance with our model, formation of consortia of ANME and DSS may have a significant effect on sulfur isotope fractionation, and the disulfide concentration is expected to be much lower than the concentrations of sulfate and hydrogen sulfide, which could make difficult quantitative experimental assessment of the disulfide concentration.

If biomass is not considered, Equations (2) and (3) transform into:

$$7CH_4 + 8SO_4^{2-} = 4HS_2^- + 7HCO_3^- + 6H_2O + 5OH^- \quad (4)$$

$$4HS_2^- + 4H_2O = SO_4^{2-} + 7HS^- + 5H^+ \quad (5)$$

and the overall reaction becomes:

$$CH_4 + SO_4^{2-} = HS^- + HCO_3^- + H_2O \quad (6)$$

which is similar to that given in Knittel & Boetius (2009).

The traditional description of reversible AOM-SR dynamics

First, we introduce the Monod functions with two substrates similar to Batstone *et al.* (2002) describing the rates R (forward reaction) and R^{rev} (reverse reaction) in (2) and (3):

$$R_{ANME} = \rho_{mANME} B_{ANME} \frac{CH_4}{K_{CH4} + CH_4} \frac{SO_4^{2-}}{K_{SO_4^{2-}} + SO_4^{2-}} \quad (7)$$

$$R_{DSS} = \rho_{mDSS} B_{DSS} \frac{HS_2^-}{K_{HS_2^-} + HS_2^-} \frac{HCO_3^-}{K_{HCO_3^-} + HCO_3^-} \quad (8)$$

$$R^{rev}_{ANME} = \rho^{rev}_{mANME} B_{ANME} \frac{HCO_3^-}{K^{rev}_{HCO_3^-} + HCO_3^-} \frac{HS_2^-}{K^{rev}_{HS_2^-} + HS_2^-} \quad (9)$$

$$R^{rev}_{DSS} = \rho^{rev}_{mDSS} B_{DSS} \frac{HS^-}{K^{rev}_{HS^-} + HS^-} \frac{SO_4^{2-}}{K^{rev}_{SO_4^{2-}} + SO_4^{2-}} \quad (10)$$

where HS_2^- and HS^- are the disulfide and hydrogen sulfide concentrations; B_{ANME} and B_{DSS} are the active ANME and DSS biomass concentrations; ρ_{mANME}, ρ_{mDSS}, ρ^{rev}_{mANME}, and ρ^{rev}_{mDSS} are the maximum specific forward and reverse rates of substrate consumption; K_{CH_4}, $K_{SO_4^{2-}}$, $K_{HCO_3^-}$, $K_{HS_2^-}$, $K^{rev}_{SO_4^{2-}}$, $K^{rev}_{HCO_3^-}$, $K^{rev}_{HS^-}$ and $K^{rev}_{HS_2^-}$ are the corresponding half-saturation coefficients. It is supposed that NH_4^+ is in excess in the reactor. Assuming that all chemical reagents are uniformly distributed over the reactor volume, while the biomass is located at the bottom, being washed out only slightly, the general model of the continuous-flow reactor carrying out reversible AOM-SR can be written as follows:

$$\begin{aligned}
\frac{dCH_4}{dt} &= -R_{ANME} + \frac{1}{T}(CH_4^{in} - CH_4) \\
\frac{dSO_4^{2-}}{dt} &= -\frac{8 - (20 - x)\,Y_{ANME}}{7}(R_{ANME} - R^{rev}_{ANME}) \\
&\quad + \frac{1 + (20 - z)Y_{DSS}}{7}(R_{DSS} - R^{rev}_{DSS}) \\
&\quad + \frac{1}{T}(SO_4^{2-\,in} - SO_4^{2-}) \\
\frac{dHCO_3^-}{dt} &= (1 - 5Y_{ANME})(R_{ANME} - R^{rev}_{ANME}) \\
&\quad - 5Y_{DSS}(R_{DSS} - R^{rev}_{DSS}) + \frac{1}{T}(HCO_3^{-\,in} - HCO_3^-) \\
\frac{dHS_2^-}{dt} &= \frac{4 - (10 + 3x)Y_{ANME}}{7}(R_{ANME} - R^{rev}_{ANME}) \\
&\quad - \frac{4 + (10 + 3z)Y_{DSS}}{7}(R_{DSS} - R^{rev}_{DSS}) \\
&\quad + \frac{1}{T}(HS_2^{-\,in} - HS_2^-) \\
\frac{dHS^-}{dt} &= R_{DSS} - R^{rev}_{DSS} + \frac{1}{T}(HS^{-\,in} - HS^-)
\end{aligned} \quad (11)$$

$$\begin{aligned}
\frac{dB_{ANME}}{dt} &= Y_{ANME}(R_{ANME} + R^{rev}_{ANME}) \\
&\quad - k_{dANME}B_{ANME} + \frac{1}{T_b}(B^{in}_{ANME} - B_{ANME}) \\
\frac{dB_{DSS}}{dt} &= Y_{DSS}(R_{DSS} + R^{rev}_{DSS}) - k_{dDSS}B_{DSS} + \frac{1}{T_b}(B^{in}_{DSS} - B_{DSS})
\end{aligned} \quad (12)$$

where Y_{ANME}, Y_{DSS} and $k_{d\,ANME}$, $k_{d\,DSS}$ are the biomass yield coefficients and the biomass decay coefficients of ANME and DSS, respectively; T and T_b are the retention times of the soluble reagents and biomass, respectively. It is assumed that the

biomass of microorganisms was washed out of the reactor extremely slowly, with $T_b = 1{,}000\ \mathrm{d} >> T = 0.6\ \mathrm{d}$. The superscript 'in' denotes the incoming concentration of the reagent. Polymerization of hydrogen disulfide HS_2^- is not taken into account in the system of Equations (11) and (12).

Taking into account that the rate of concentration changes of heavier substrates, products, and biomasses is proportional to the rate of concentration changes of the total (light + heavier) substrates, products and biomasses, the system of Equations (11) and (12) is supplemented by the corresponding equations for 'heavier' sulfur in the forward and reverse reactions:

$$\frac{d\,{}^{34}SO_4^{2-}}{dt} = \frac{1}{\alpha_{S\text{-}SO_4^{2-}}}\frac{8-(20-x)Y_{ANME}}{7}\left(-\frac{{}^{34}SO_4^{2-}}{SO_4^{2-}}R_{ANME} + \frac{H^{34}S_2^-}{HS_2^-}R_{ANME}^{rev}\right) + \frac{1}{\alpha_{S-HS_2^-}}\frac{1+(20-z)\,Y_{DSS}}{7}\left(\frac{H^{34}S_2^-}{HS_2^-}R_{DSS} - \frac{{}^{34}SO_4^{2-}}{SO_4^{2-}}R_{DSS}^{rev}\right) + \frac{1}{T}\left({}^{34}SO_4^{2-\,\mathrm{in}} - {}^{34}SO_4^{2-}\right) \quad (13)$$

$$\frac{d\,H^{34}S_2^-}{dt} = \frac{1}{\alpha_{S\text{-}SO_4^{2-}}}\frac{4-(10+3x)\,Y_{ANME}}{7}\left(\frac{{}^{34}SO_4^{2-}}{SO_4^{2-}}R_{ANME} - \frac{H^{34}S_2^-}{HS_2^-}R_{ANME}^{rev}\right) - \frac{1}{\alpha_{S\text{-}HS_2^-}}\frac{4+(10+3z)\,Y_{DSS}}{7}\left(\frac{H^{34}S_2^-}{HS_2^-}R_{DSS} - \left(\frac{{}^{34}SO_4^{2-}}{SO_4^{2-}} + \frac{{}^{34}HS^-}{HS^-}\right)R_{DSS}^{rev}\right) + \frac{1}{T}(H^{34}S_2^{-\,\mathrm{in}} - H^{34}S_2^-) \quad (14)$$

$$\frac{d\,H^{34}S^-}{dt} = \frac{1}{\alpha_{S\text{-}HS_2^-}}\frac{H^{34}S_2^-}{HS_2^-}R_{DSS} - \frac{1}{\alpha_{S\text{-}HS_2^-}}\frac{{}^{34}HS^-}{HS^-}R_{DSS}^{rev} + \frac{1}{T}(H^{34}S^{-\,\mathrm{in}} - H^{34}S^-) \quad (15)$$

$$\frac{d^{34S}B_{ANME}}{dt} = \frac{1}{\alpha_{S\text{-}SO_4^{2-}}}Y_{ANME}\left(\frac{{}^{34}SO_4^{2-}}{SO_4^{2-}}R_{ANME} + \frac{H^{34}S_2^-}{HS_2^-}R_{ANME}^{rev}\right) - k_{dANME}\,{}^{34S}B_{ANME} + \frac{1}{T_b}({}^{34S}B_{ANME}^{in} - {}^{34S}B_{ANME}) \quad (16)$$

$$\frac{d^{34S}B_{DSS}}{dt} = \frac{1}{\alpha_{S\text{-}HS_2^-}}Y_{DSS}\left(\frac{H^{34}S_2^-}{HS_2^-}R_{DSS} + \left(\frac{{}^{34}SO_4^{2-}}{SO_4^{2-}} + \frac{{}^{34}HS^-}{HS^-}\right)R_{DSS}^{rev}\right) - k_{dDSS}\,{}^{34S}B_{DSS} + \frac{1}{T_b}({}^{34S}B_{DSS}^{\mathrm{in}} - {}^{34S}B_{DSS}) \quad (17)$$

where ${}^{34}SO_4^{2-}$, $H^{34}S_2^-$ and $H^{34}S^-$ are the concentrations of heavier sulfur reagents, ${}^{34S}B_{ANME}$ and ${}^{34S}B_{DSS}$ are the concentrations of the biomass enriched in heavier sulfur, $\alpha_{S\text{-}SO_4^{2-}}$ and $\alpha_{S\text{-}HS_2^-}$ are the corresponding sulfur isotope fractionation factors.

Formation of ANME + DSS consortium in the process of AOM-SR

First, we introduce an equation for the concentration of consortium with biomass inside consortia C_S:

$$\frac{dC_S}{dt} = k\,B_{ANME}^{free}B_{DSS}^{free} - k_d\,C_S + R_{ANME}^{C_S} + R_{ANME}^{CSrev} + R_{DSS}^{C_S} + R_{DSS}^{CSrev} \quad (18)$$

where k is a coefficient characterizing the rate of consortia formation; k_d is the consortia decay rate coefficient; B_{ANME}^{free} and B_{DSS}^{free} are the active free-swimming ANME and DSS biomass concentrations. Due to the growth of ANME and DSS biomasses during AOM-SR, the value of C_S increases.

Instead of functions (7)–(10), the following rate functions can be used in (18):

$$R_{ANME}^{C_S} = \rho_{mANME}\,\beta\,C_S\,\frac{CH_4}{K_{CH4}+CH_4}\,\frac{SO_4^{2-}}{K_{SO_4^{2-}}+SO_4^{2-}} \quad (19)$$

$$R_{DSS}^{C_S} = \rho_{mDSS}\,(1-\beta)\,C_S\frac{HS_2^-}{K_{HS_2^-}+HS_2^-}\frac{HCO_3^-}{K_{HCO_3^-}+HCO_3^-} \quad (20)$$

$$R_{ANME}^{CSrev} = \rho_{mANME}^{rev}\,\beta\,C_S\,\frac{HCO_3^-}{K_{HCO_3^-}^{rev}+HCO_3^-}\frac{HS_2^-}{K_{HS_2^-}^{rev}+HS_2^-} \quad (21)$$

$$R_{DSS}^{CSrev} = \rho_{mDSS}^{rev}(1-\beta)C_S\frac{HS^-}{K_{HS^-}^{rev}+HS^-}\,\frac{SO_4^{2-}}{K_{SO_4^{2-}}^{rev}+SO_4^{2-}} \quad (22)$$

where $\beta\,C_S$ and $(1-\beta)\,C_S$ are the respective concentrations of ANME and DSS biomasses inside the consortium.

In the rate functions (19)–(22), the concentration of consortium C_S is written instead of the biomass concentrations of ANME and DSS. Now, in (7)–(10)

$$B_{ANME} = B_{ANME}^{free} + \beta\,C_S$$
$$B_{DSS} = B_{DSS}^{free} + (1-\beta)\,C_S \quad (23)$$

For free-swimming biomasses the following equations are used instead of (12):

$$\frac{dB_{ANME}^{free}}{dt} = Y_{ANME}\frac{B_{ANME}^{free}}{B_{ANME}}(R_{ANME}+R_{ANME}^{rev}) - k_{d\,ANME}B_{ANME}^{free} + \frac{1}{T_b}(B_{ANME}^{in}-B_{ANME}^{free})$$

$$\frac{dB_{DSS}^{free}}{dt} = Y_{DSS}\frac{B_{DSS}^{free}}{B_{DSS}}(R_{DSS}+R_{DSS}^{rev}) - k_{d\,DSS}B_{DSS}^{free} + \frac{1}{T_b}(B_{DSS}^{in}-B_{DSS}^{free}) \quad (24)$$

The proportion of ANME and DSS in consortium (β) is considered constant and used as one of the model's parameters. Evidently, the possibility of sulfate molecules to contact with cells in a consortium depends on the concentration of consortia C_S. A mean distance between a typical consortium and sulfate molecules decreases at higher C_S. Thus, it can be assumed that the value of fractionation factor α will be lower at higher C_S.

Both schemes of AOM + SR are shown in Figure 1. All numerical simulations were performed using the MATLAB Software (MathWorks Inc. 1984). Values of the coefficients used in the model are presented in Table 1. Similar to Vavilin *et al.* (2017), the model calibration process was

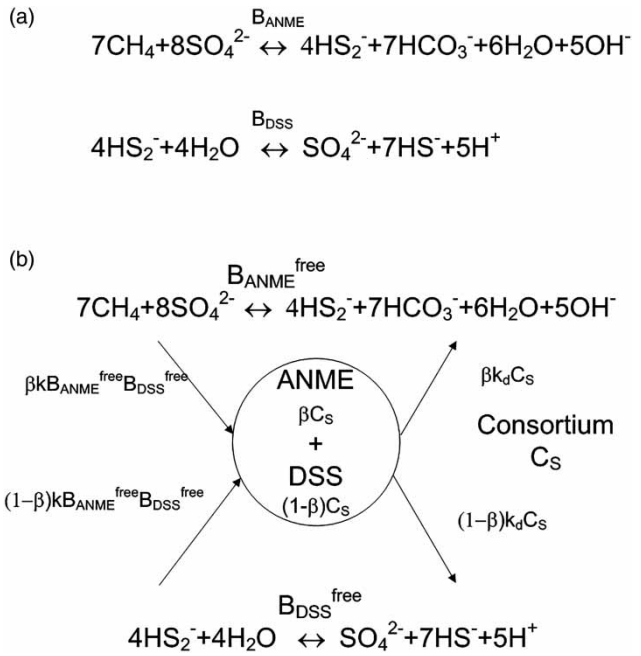

Figure 1 | Two schemes of AOM-SR: traditional (a) and non-traditional with consortium of ANME + DSS (b).

Table 1 | Sulfur isotope fractionation factors α_S and initial free-swimming biomass B_0 of ANME and DSS and consortia C_{S0} concentrations[a]

Process	Influent sulfate, mM	B_0, mM	C_{S0}, mM	α_S
Figure 2				
Influent $CH_4 = 3.3$ mM	7.4			
ANME		2.2		1.035
DSS		2.2		1.035
Figure 3				
Influent $CH_4 = 26$ mM	7.0			
ANME		7.5		1.018
DSS		7.5		1.018
Figure 4[b]				
Influent $CH_4 = 3.3$ mM	7.4		1.5	
ANME		1.2		1.04
DSS		1.0		1.04
Figure 5[b]				
Influent $CH_4 = 8$ mM	7.0		3.5	
ANME		2.0		1.024
DSS		1.4		1.024
Figure 6[b]				
Influent $CH_4 = 14$ mM	7.0		7.0	
ANME		2.4		1.023
DSS		1.8		1.023
Figure 7[b]				
Influent $CH_4 = 26$ mM	6.5		7.5	
ANME		3.0		1.022
DSS		2.1		1.022
Figure 8[b]				
Influent $CH_4 = 44$ mM	9.0		12.0	
ANME		3.5		1.018
DSS		2.4		1.018

Reversible reactions are not presented. In computer simulations, mol L^{-1} units were used for concentrations.

[a]In the model, in all figures for ANME and DSS the same biomass yield coefficients $Y = 0.05$ mmol $mmol^{-1}$, the biomass decay coefficients for ANME and DSS $k_{d\,ANME} = 0$ and $k_{d\,DSS} = 0$, the half-saturation coefficients $K_{CH_4} = 0.5$ mM, $K_{SO_4^{2-}} = 0.5$ mM, $K_{HCO_3^-} = 0.01$ mM, $K_{HS_2^-} = 0.001$ mM, and the maximum specific biomass growth rate $\mu_m^{ANME} = Y^{ANME}\rho_m^{ANME} = 0.020\,d^{-1}$ and $\mu_m^{DSS} = Y^{DSS}\rho_m^{ANME} = 0.018\,d^{-1}$ were used. Biomass decay was not taken into account.

[b]In Figures 4–8, consortium formation growth and decay coefficients $k = 10$ mM^{-1} d^{-1}, $k_d = 10\,d^{-1}$ were used. The value of $\beta = 0.48$ was used for consortium.

divided into two parts. First, calibration was performed for non-isotopic data (methane, sulfate and hydrogen sulfide dynamic curves). Second, the isotopic data ($\delta^{34}S$ dynamic changes in sulfate and hydrogen sulfide) were used in the calibration process. The sulfur isotope signature is

calculated using the next equation:

$$\delta^{34S}Q\,[‰] = \left[\frac{^{34S}Q/(Q - {}^{34S}Q)}{0.0112372} - 1\right], \quad (25)$$

where ^{34S}Q and Q are the concentrations of heavier and total sulfur components, respectively.

RESULTS AND DISCUSSION

The conventional description of AOM-SR dynamics

Figures 2 and 3 demonstrate the system dynamics at low (3.3 mM) and high (26 mM) influent methane concentrations. The model parameters are shown in Table 1. The initial active biomass concentration (Figure 2(c)) is less than the cell weight concentration (4.6 g_{DW} L^{-1}) measured by Deusner *et al.* (2014). As $T_d = \ln 2/\mu_m$ (T_d, biomass doubling time; μ_m, maximum specific biomass growth rate), the biomass doubling time in the model is 35 d for ANME and 39 d for DSS. Concentrations of ANME and DSS are slowly increasing during incubation (Figures 2(c) and 3(c)). The concentration of intermediate product HS_2^- is much lower than the concentration of substrate (SO_4^{2-}) (Figures 2(b) and 3(b)). Soon after the start, the hydrogen disulfide concentration reaches a steady-state value when the production of HS_2^- becomes approximately equal to its consumption. It can be concluded that AOM is the rate-limiting reaction and the system dynamics is not in a true steady state due to the continuous biomass accumulation (Figures 2(c) and 3(c)).

Deusner *et al.* (2014) evaluated sulfur isotope fractionation in the reaction (1) using simple balance Equations (4) and (5) that did not consider biomass. It was shown that the smallest sulfur and oxygen isotope fractionation was observed for the highest influent methane concentration with the highest AOM-SR rate. In accordance with our dynamic model that takes into account biomass accumulation, the sulfur isotope fractionation may occur in both reactions of AOM and SR. In agreement with experimental data, the dynamic model shows that the sulfur isotope fractionation factors are lower at higher influent methane concentration (Figure 2(e) and 2(f), Figure 3(e) and 3(f)), which corresponds to a higher biomass concentration. When biomass accumulation was not considered, a relatively high AOM rate at increasing of influent methane concentration cannot be obtained. The model demonstrates that the system dynamics depends weakly on the ratio of S/C in the biomass (not shown).

Correct measurement of active biomass concentration in experiments is often problematic. Traditional models of microbial dynamics are based on writing equations for the consumption and production rates of different chemical

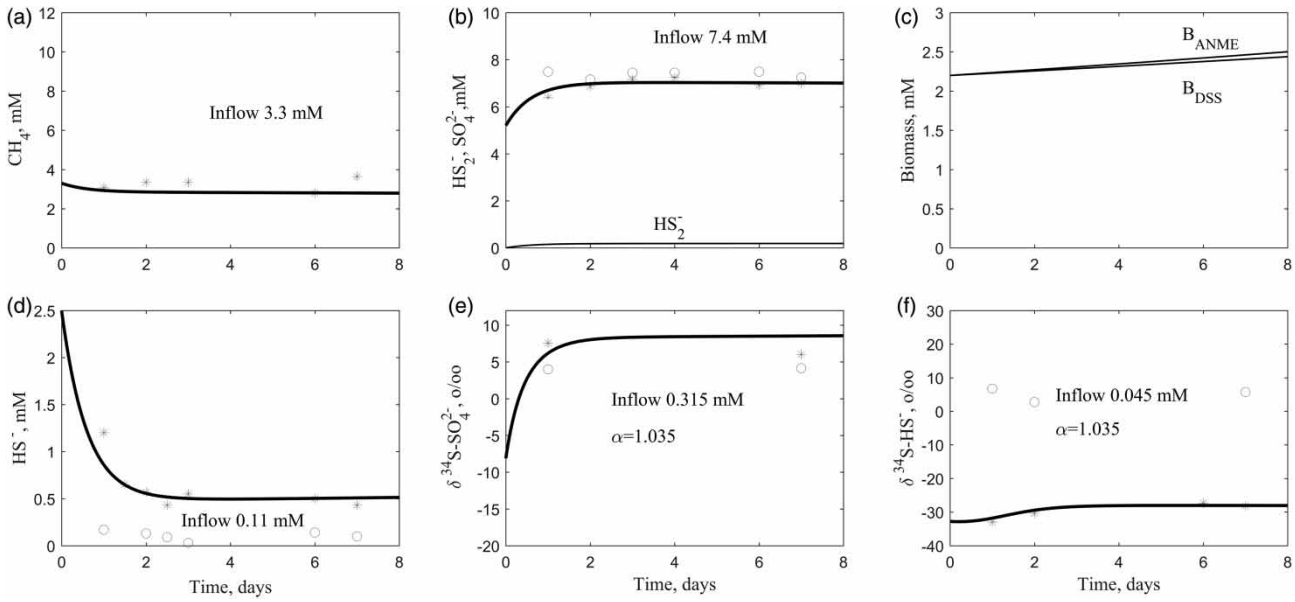

Figure 2 | System dynamics of AOM-SR at a low influent methane concentration of 3.3 mM. Symbols: experimental data (Deusner *et al.* 2014); curves: traditional model. Panels: influent (open symbols) and effluent (asterisks) reagent concentrations. Curves: (a) effluent methane concentration; (b) effluent sulfate and hydrogen disulfide concentrations; (c) effluent biomass concentrations of free-swimming ANME and DSS; (d) effluent hydrogen sulfide concentration; (e) effluent isotope signatures (25) of sulfate; (f) effluent isotope signatures (25) of hydrogen sulfide. α – sulfur isotope fractionation factor. In the panels, the respective influent reagent concentrations used in the model are written (inflow).

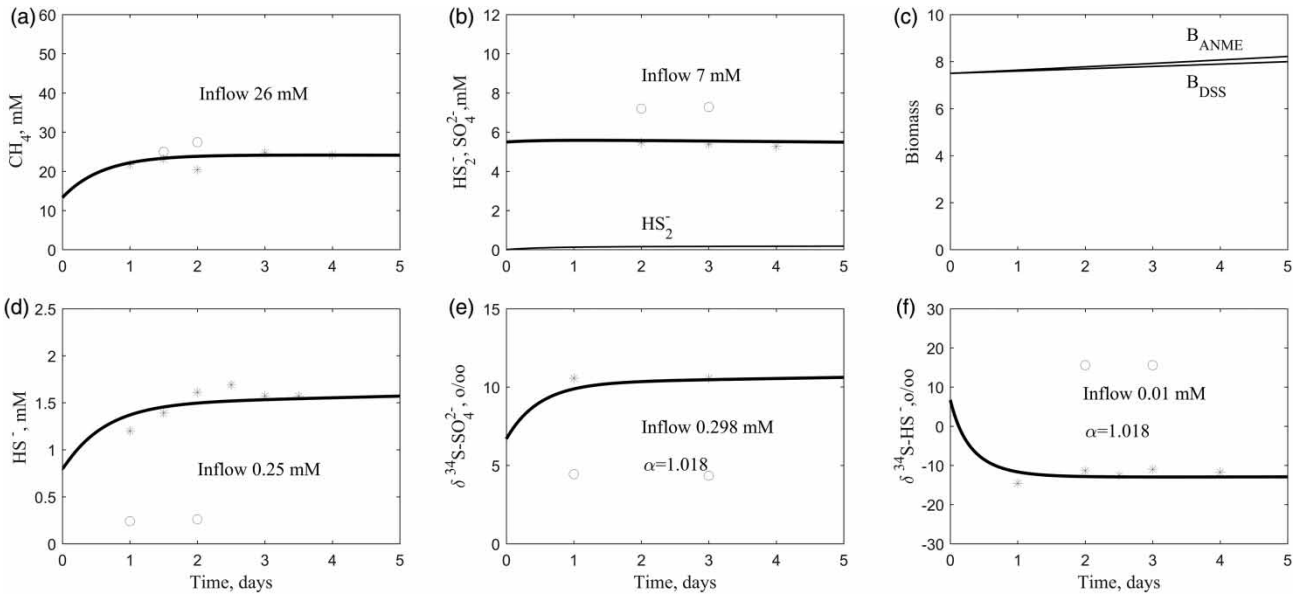

Figure 3 | System dynamics of AOM-SR at a high influent methane concentration of 26 mM. Symbols: experimental data (Deusner *et al.* 2014); curves: traditional model. Panels: influent (open symbols) and effluent (asterisks) reagent concentrations. See caption to Figure 2.

and biological components and the concentrations of those components. A decrease in biomass concentration is generally compensated for by an increase in the value of ρ_m to have approximately the same substrate consumption and product formation rates (similar model adequacy) in the Monod functions (7)–(10). In accordance with the rate functions (7)–(10) of ANME and DSS, instead of the assumption of biomass accumulation, the respective increase in the maximum specific biomass growth rates μ_m of ANME and DSS may be assumed. The model shows that experimental data are described well without considering a reversible character of AOM and DSS.

From the results presented in Figures 2 and 3 we can postulate that different microbial species of ANME and DSS can be responsible for the variability of α_S. However, this assumption is rather unlikely because the sulfur isotope fractionation factor proved to be the same for ANME and DSS. Also, if the maximum biomass growth rate of ANME is somewhat higher than that of DSS, the concentration of ANME during a long incubation should be higher than that of DSS. It is contradictory to the results shown in Figures 2(c) and 3(c) with the same initial concentration of both biomasses. During sequential incubations at the time interval between 46 and 117 days (Deusner *et al.* 2014), in accordance with the model, a high increase of the biomass concentrations of ANME and DSS from 2.2 to 7.5 mM (Table 1) should be assumed that is not possible with the biomass doubling time equal to 35 d (ANME) and 39 d (DSS). Similar conclusions were obtained from the other influent methane concentrations of 8, 14.9, and 43 mM (not shown).

The biomass performing AOM-SR consists of active biomass, inactive or non-AOM-SR cells, extracellular polymeric substances and carbonate precipitates (Michaelis *et al.* 2002; Deusner *et al.* 2014). Very slow biomass growth rates with a biomass doubling time (T_d) up to a few months were reported in a number of studies (Girguis *et al.* 2005; Nauhaus *et al.* 2007; Wegener 2008; Orphan *et al.* 2009). For batch experiments, biomass doubling time depends on the value of the half-saturation constant K_S for methane (Wegener 2008). Based on the Rayleigh equation, Holler *et al.* (2009) showed that the isotope fractionation factors α_C and α_H for $\delta^{13}CH_4/\delta^{12}CH_4$ and $\delta CDH_3/\delta CH_4$ from duplicate experiments were 1.012 and 1.12 (Hydrate Ridge: 12 °C), 1.02 and 1.2 (Amon Mud Volcano: 20 °C) and 1.036 and 1.34 (microbial mat from the Black Sea: 12 °C), respectively. For the microbial mat from the Black Sea, the highest fractionation factors α_C and α_H were obtained at lowest specific methane consumption rate. Holler *et al.* (2009) suggested that different microbial species could be responsible for the variability of α_C and α_H.

From the Monod functions (7)–(10), it should be noted that, during calibration, a higher value of T_d may be obtained when lower values of μ_m were assumed. In that case, during model calibration, higher values of initial biomass concentrations of ANME and DSS have to be used.

The significance of ANME + DSS consortium in the process of AOM-SR

Besides microbial species, diffusion limitation as well as different reversibility in the enzymatic steps may affect methane consumption rate, which, in turn, may lead to the observed difference of isotope fractionation (Valentine *et al.* 2004; Holler *et al.* 2011; Thauer 2011). Milucka *et al.* (2012) reported that ANME reduces sulfate to zero-valent sulfur during methane oxidation while DSS gains energy from disulfide disproportionation, and that AOM coupled with SR becomes energetically more favorable if the disulfide produced is scavenged. Evidently, in the microbial consortium of ANME + DSS, the overall process has a low energy output (Equation (1)) which is shared between ANME and DSS. The model describing consortium formation shows that experimental data are described well without considering a reversible character of AOM and DSS.

Figures 4–8 demonstrate the system dynamics with the formation of consortia at the different influent methane concentrations and at the same rate constant k of consortium formation. The model parameters are shown in Table 1. The specific biomass growth rates of ANME and DSS are assumed to be similar to those used in Figures 2 and 3. In the model, a single isotope fractionation factor is used for ANME and DSS. A process of AOM-SR stops at $C_S = 0$ (not shown). The biomass concentrations of free-swimming ANME and DSS are significantly less for the non-traditional model (18) than for the model not considering the formation of consortia (compare Figures 7(c) and 3(c)). The model demonstrates that the increasing concentration of consortia is adjusted to the current values of biomass concentrations of ANME and DSS (not shown). The concentration of product (HS^-) as well as its isotope signature (δ^{34}S-HS^-) increases at the higher influent methane concentration.

The formation rate of the ANME + DSS consortia which is much higher than the biomass growth rates of free-swimming microorganisms is significantly higher at higher influent methane concentration (compare part (c) of Figures 4–8) causing a strong decrease of the current concentration of HS_2^- (part (b), Figures 4–8). In accordance with the model, AOM is the rate-limiting stage in the total process of AOM-SR, where the influent concentration of dissolved methane was significantly increased from 3.3 to 44 mM, while the influent concentration of sulfate was only in the range from 6.5 to 9.0 mM. Evidently, a limitation in sulfate concentration decreases the rate of AOM (Equations (7) and (19)).

The greater is the concentration of microbial consortia, the smaller the average distance between microorganisms

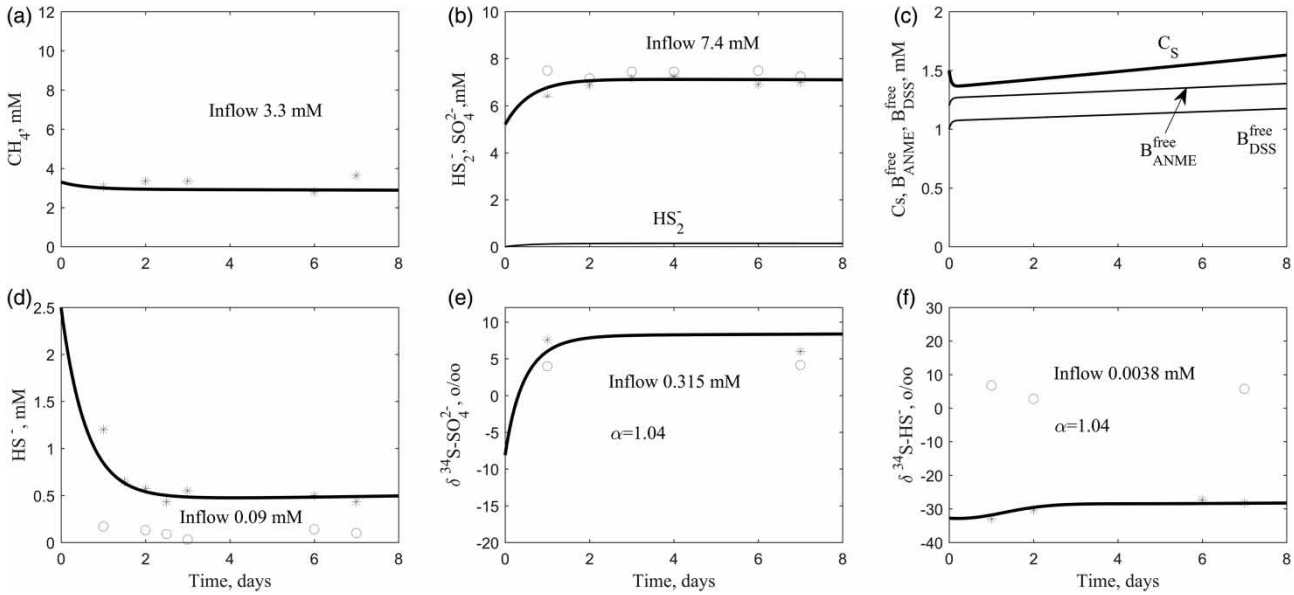

Figure 4 | System dynamics of AOM-SR at the influent methane concentration of 3.3 mM. Symbols: experimental data (Deusner *et al.* 2014); curves: non-traditional model that takes into account consortium formation. Panels: influent (open symbols) and effluent (asterisks) reagent concentrations. Curves: (c) consortium C_S and free-swimming ANME and DSS concentrations; curves of other panels are as given in caption to Figure 2.

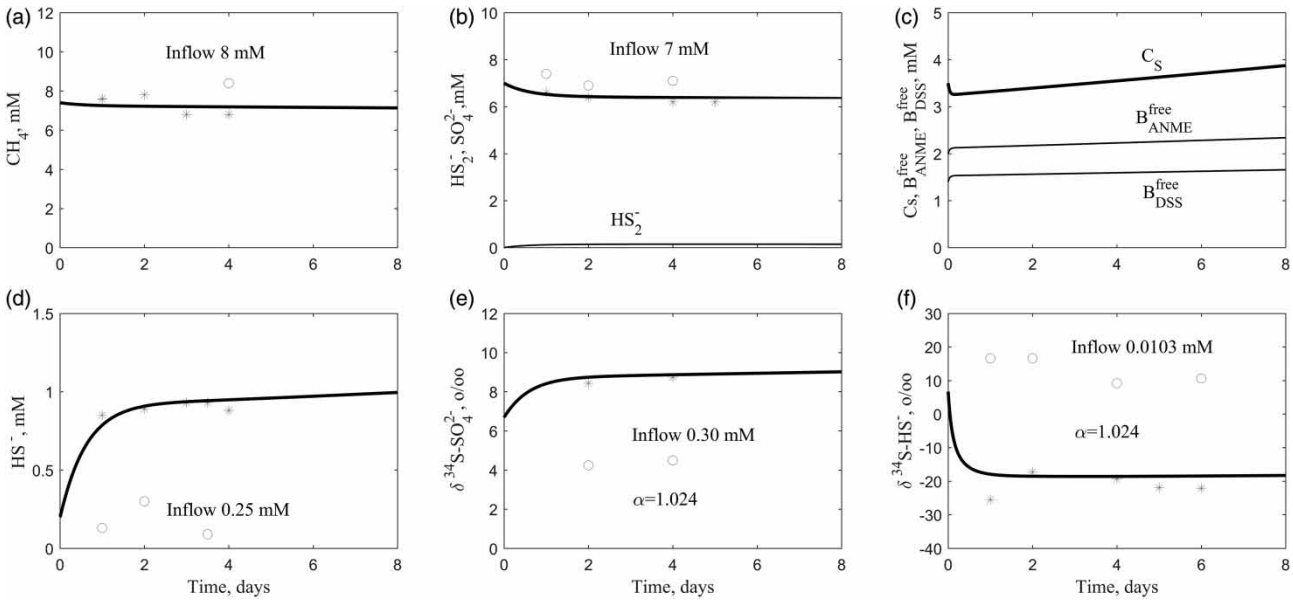

Figure 5 | System dynamics of AOM-SR at the influent methane concentration of 8 mM. Symbols: experimental data (Deusner *et al.* 2014); curves: non-traditional model that takes into account consortium formation. Panels: influent (open symbols) and effluent (asterisks) reagent concentrations. See captions to Figures 2 and 4.

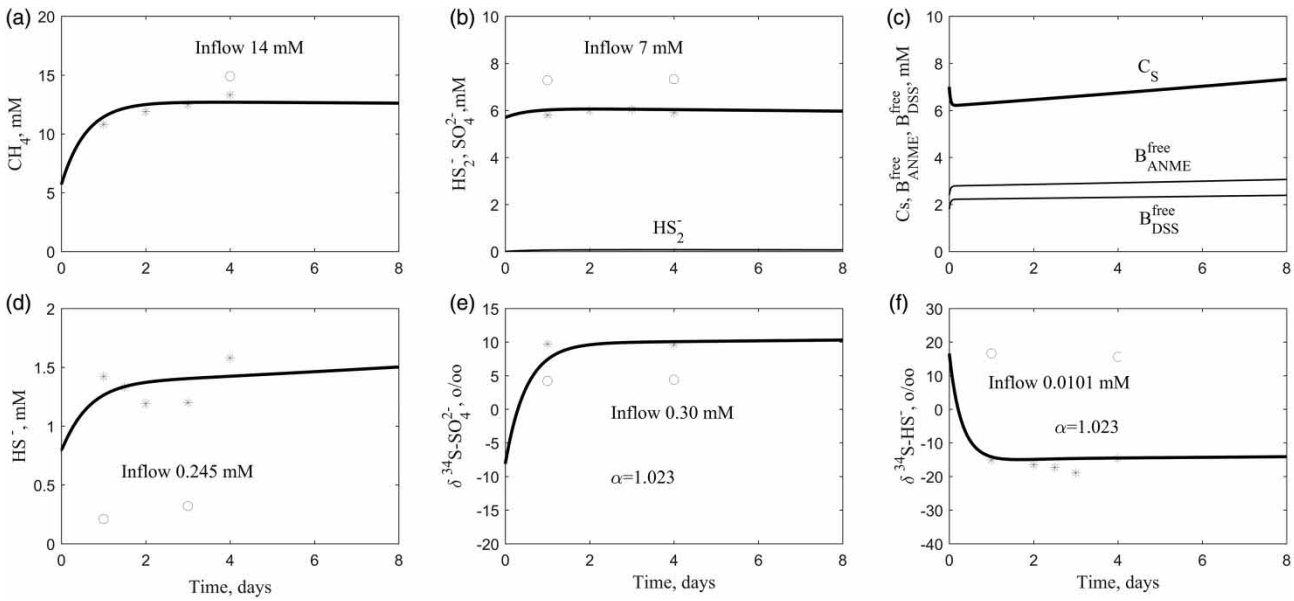

Figure 6 | System dynamics of AOM-SR at the influent methane concentration of 14.9 mM. Symbols: experimental data (Deusner *et al.* 2014); curves: non-traditional model that takes into account consortium formation. Panels: influent (open symbols) and effluent (asterisks) reagent concentrations. See captions to Figures 2 and 4.

and sulfur-containing molecules (SO_4^{2-}, HS_2^-). This fact, in turn, because of diffusion, may lead to the lower sulfur isotope fractionation. According to Deusner *et al.* (2014), at the lowest influent methane concentration (1.4 ± 0.6 mM) a high scatter in the isotope signature values was observed. Taking into account that in this case the concentration of consortia was lowest, quite different consortium concentrations may be in the different samples taken from non-perfect mixing solution.

It should be noted that at a very low concentration of HS_2^- a variation of the isotope fractionation factor for SR is not important while the isotope fractionation factor for AOM has a dominant effect on the sulfur isotope dynamics.

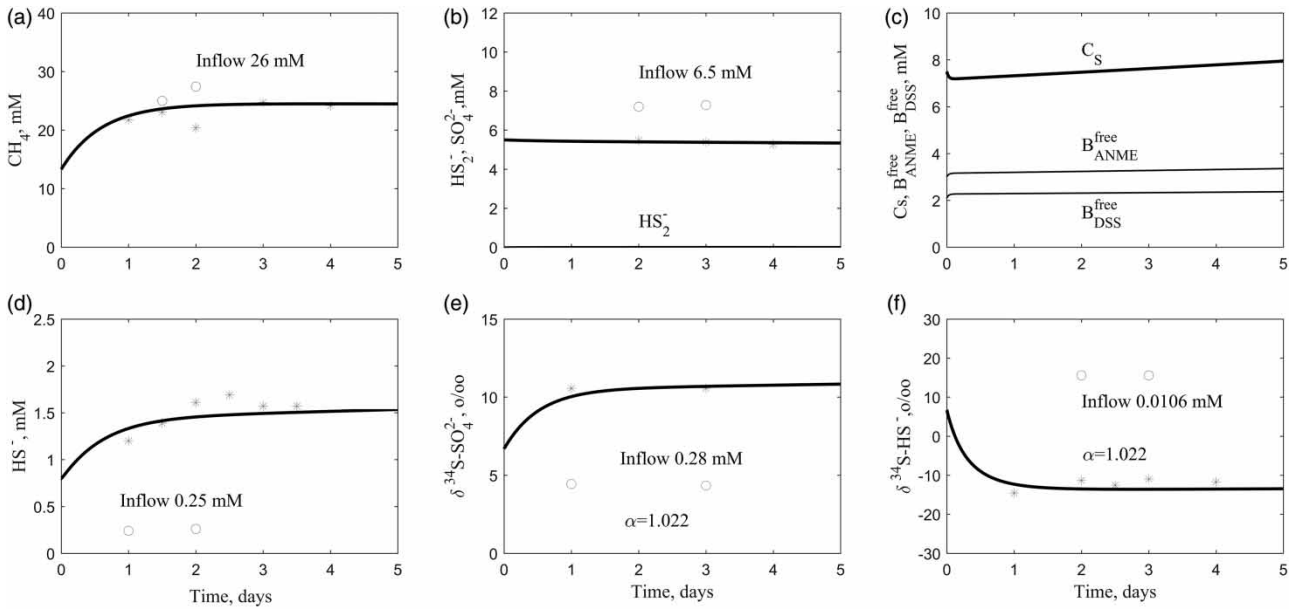

Figure 7 | System dynamics of AOM-SR at the influent methane concentration of 26 mM. Symbols: experimental data (Deusner *et al.* 2014); curves: non-traditional model that takes into account consortium formation. Panels: influent (open symbols) and effluent (asterisks) reagent concentrations. See captions to Figures 2 and 4.

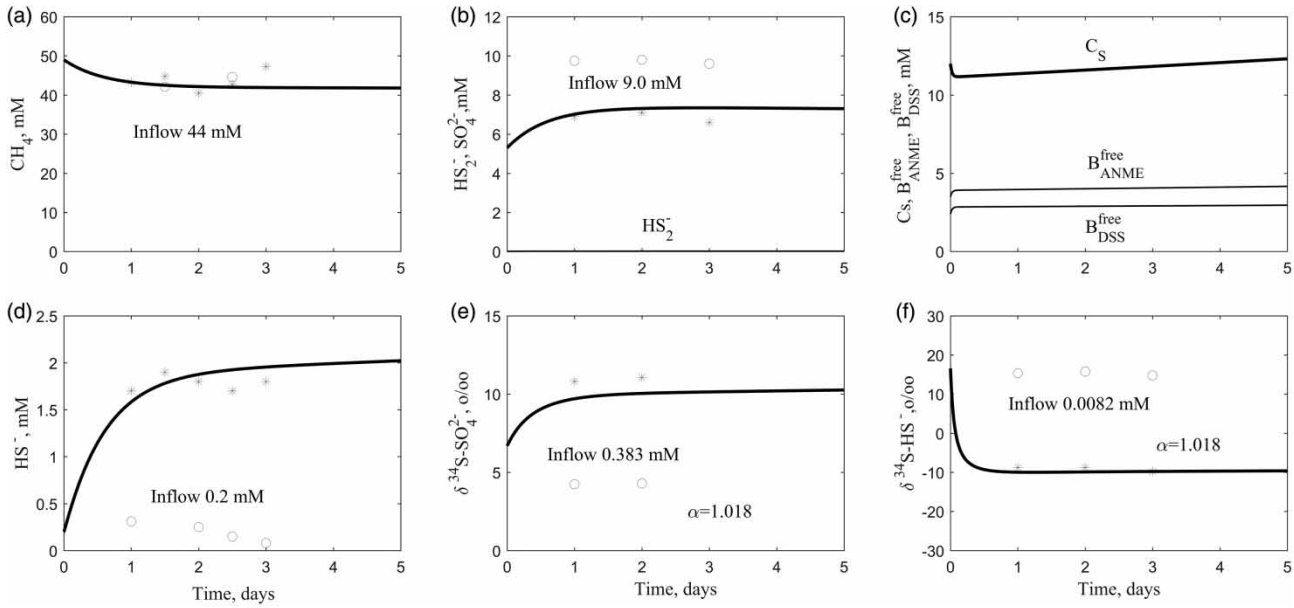

Figure 8 | System dynamics of AOM-SR at the influent methane concentration of 43 mM. Symbols: experimental data (Deusner *et al.* 2014); curves: non-traditional model that takes into account consortium formation. Panels: influent (open symbols) and effluent (asterisks) reagent concentrations. See captions to Figures 2 and 4.

CONCLUSIONS

- Two dynamic models of reversible methane oxidation by ANME and sulfate reduction by DSS, that took into account biomass growth and included sulfur isotope variables without and with formation of microbial consortia, were developed to describe Deusner's experimental data of continuous-flow laboratory incubations. In both the models, if biomass was not considered, relatively high AOM rate at a higher influent methane concentration could not be obtained.

- Disulfide formation as an intermediate product during AOM and SR is considered in the models based on the stoichiometry with sulfur element. The models predict that the concentration of intermediate product HS_2^- is much less than that of SO_4^{2-}. It can be concluded that AOM is the rate-limiting reaction and the system dynamics is not in a true steady state due to continuous biomass accumulation. Similar sulfur isotope fractionation occurred in both reactions of AOM and SR.
- In the models, the biomass doubling time of ANME and DSS is equal to 35*d* and 39*d*, respectively. ANME and DSS are slowly growing microorganisms. The models demonstrate that the dynamics of the system is marginally affected by the ratio of S/C in biomass and that introduction of reversibility of the AOM and SR reactions cannot improve the model fit to experimental data.
- A dynamic model of AOM-SR that considers a formation of consortia of ANME + DSS is proved to be more appropriate to describe system dynamics. In accordance with the model, the system dynamics may be interpreted as a significant increase in the concentration of ANME + DSS consortia at a higher influent methane concentration, which may lead to lower sulfur isotope fractionation factors due to the shorter average distance between microbial consortia of ANME + DSS and the respective sulfur substrates (SO_4^{2-}, HS_2^-).
- Finally, it should be noted that, despite the offered dynamic model being rather complex, it substantially reduces the overall complexity of reactions involved in AOM and SR, highlighting the most critical steps. Obviously, the set of parameters used in our model is not unique, as some of the parameters mutually influence each other. For example, in order to fit the model, higher initial concentrations of microorganisms can be compensated for by a decrease of their maximum specific growth rates. Although a 'correct' description of the microbial consortium formation needs knowledge of the actual ratio of ANME and DSS biomasses, changes in the value of this parameter within reasonable limits would not affect the major conclusion done on the basis of our model that the fractionation of sulfur isotopes in the course of AOM-SR is inversely proportional to the rate of formation of ANME + DSS consortia which coincides with an increase of the total reaction rate.

FUNDING

The work was supported by the Russian Science Foundation (project no. 17-17-01204).

REFERENCES

Batstone, D. J., Keller, J., Angelidaki, I., Kalyuzhnyi, S. V., Pavlosthatis, S. G., Rozzi, A., Sanders, W. T. M., Siegrist, H. & Vavilin, V. A. 2002 *Anaerobic Digestion Model No. 1 (ADM1)*. IWA Publishing, UK.

Beal, E. J., Claire, M. W. & House, C. H. 2011 High rates of anaerobic methanotrophy at low sulphate concentrations with implications for past and present methane levels. *Geobiology* **9** (2), 131–139.

Boetius, A., Ravenschlag, K., Schubert, S. J., Rickert, D., Widdel, F., Gieseke, A., Aman, R., Jorgensen, B. B., Whitte, U. & Pfannkuche, O. 2000 A marine microbial consortium apparently mediated anaerobic oxidation of methane. *Nature* **407** (6804), 623–626.

Deusner, C., Holler, T., Arnold, G. L., Bernasconi, S. M., Formolo, M. J. & Brunner, B. 2014 Sulfur and oxygen isotope fractionation during sulfate reduction coupled to anaerobic oxidation of methane is dependent on methane concentration. *Earth Planet. Sci. Lett.* **399**, 61–73.

Fagerbakke, K. J., Heldal, M. & Norland, S. 1996 Content of carbon, nitrogen, oxygen, sulfur and phosphorus in native aquatic and cultured bacteria. *Aquat. Microb. Ecol.* **10**, 15–27.

Girguis, P. R., Cozen, A. E. & DeLong, E. F. 2005 Growth and population dynamics of anaerobic methane-oxidizing archaea and sulfate-reducing bacteria in a continuous-flow bioreactor. *Appl. Environ. Microbiol.* **71**, 3725–3733.

He, X., Chadwick, G., Kempes, C., Shi, Y., McGlynn, S., Orphan, V. & Meile, C. 2019 Microbial interactions in the anaerobic oxidation of methane: model simulations constrained by process rates and activity patterns. *Environ. Microbiol.* **21** (2), 631–647.

Hinrichs, K. U. & Boetius, A. 2002 The anaerobic oxidation of methane: new insights in microbial ecology and biogeochemistry. In: *Ocean Margin Systems* (G. Wefer, D. Billet, D. Hebbeln, B. Jorgensen, M. Schlüter & T. C. E. V. Weering, eds). Springer-Verlag, Berlin, pp. 457–477.

Holler, T., Wegener, G., Knittel, K., Boetius, A., Brunner, B., Kuypers, M. M. M. & Widdel, F. 2009 Substantial $\delta^{13}CH_4$/$\delta^{12}CH_4$ and *D*/*H* fractionation during anaerobic oxidation of methane by marine consortia enriched in vitro. *Environ. Microbiol. Rep.* **1** (5), 370–376.

Holler, T., Wegner, G., Niemann, H., Deusner, C., Ferdelman, T. G., Boetius, A., Brunner, B. & Widdel, F. 2011 Carbon and sulfur back flux during anaerobic microbial oxidation of methane and coupled sulfate reduction. *Proc. Natl Acad. Sci.* **108** (52), E1484–E1490.

Knittel, K. & Boetius, A. 2009 Anaerobic oxidation of methane: progress with an unknown process. *Ann. Rev. Microbiol.* **63**, 311–334.

Knittel, K., Boetius, A., Lemke, A., Eilers, H., Lochte, K., Pfannkuche, O., Linke, P. & Amann, R. 2003 Activity, distribution, and diversity of sulfate reducers and other bacteria in sediments above gas hydrate (Cascadia margin, Oregon). *Geomicrobiol. J.* **20** (4), 269–294.

MathWorks Inc. 1984 http://www.mathworks.com.

McGlynn, S. E. 2017 Energy metabolism during anaerobic methane oxidation in ANME archaea. *Microbes Environ.* **32**, 5–13.

Michaelis, W., Seifert, R., Nauhaus, K., Treude, T., Thiel, V., Blumenberg, M., Knittel, K., Gieseke, A., Peterknecht, K., Pape, T., Boetius, A., Amann, R., Jørgensen, B. B., Widdel, F., Peckmann, J., Pimenov, N. V. & Gulin, M. B. 2002 Microbial reefs in the Black Sea fueled by anaerobic oxidation of methane. *Science* **297**, 1013–1015.

Milucka, J., Ferdelman, T. G., Polerecky, L., Franzke, D., Wegener, G., Schmid, M., Lieberwirth, I., Wagner, M., Widdel, F. & Kuypers, M. M. M. 2012 Zero-valent sulphur is a key intermediate in marine methane oxidation. *Nature* **491**, 541–546.

Nauhaus, K., Albrecht, M., Elvert, M., Boetius, A. & Widdel, F. 2007 In vitro cell growth of marine archaeal-bacterial consortia during anaerobic oxidation of methane with sulfate. *Environ. Microbiol.* **9**, 187–196.

Orphan, V. J., Turk, K. A., Green, A. M. & Hous, C. H. 2009 Patterns of ^{15}N assimilation and growth of methanotrophic ANME-2 and sulfate-reducing bacteria within structured syntrophic consortia revealed by FISH-SIMS. *Environ. Microbiol.* **11** (7), 1777–1791.

Schreiber, L., Holler, T., Knittel, K., Meyerdierks, A. & Amann, R. 2010 Identification of the dominant sulfate-reducing bacterial partner of anaerobic methyanotrophs of the ANME-2 clade. *Environ. Microbiol.* **12**, 2327–2340.

Thauer, R. K. 2011 Anaerobic oxidation of methane with sulfate: on the reversibility of the reactions that are catalyzed by enzymes also involved in methanogenesis from CO_2. *Curr. Opin. Microbiol.* **14**, 292–299.

Timmers, P. H. A., Welte, C. U., Koehorst, J. J., Plugge, C. M., Jetten, M. S. M. & Stams, A. J. M. 2017 Reverse methanogenesis and respiration in methanotrophic archaea. *Archaea* **17**, 1–22. http://dx.doi.org/10.1155/2017/1654237.

Valentine, D. L., Chidthaisong, A., Rice, A., Reeburgh, W. S. & Tyler, S. C. 2004 Carbon and hydrogen isotope fractionation by moderately thermophilic methanogens. *Geochim. Cosmochim. Acta* **68** (7), 1571–1590.

Vavilin, V. A., Rytov, S. V. & Conrad, R. 2017 Modelling methane formation in sediments of tropical lakes focusing on syntrophic acetate oxidation: dynamic and static carbon isotope equations. *Ecol. Modell.* **363**, 81–95.

Vavilin, V. A., Rytov, S. V. & Lokshina, L. Y. 2018a Modelling the specific pathway of CH_4 and CO_2 formation using carbon isotope fractionation: an example for a boreal mesotrophic fen. *Isot. Environ. Health Stud.* **54**, 475–493.

Vavilin, V. A., Rytov, S. V. & Brezgunov, V. S. 2018b Basic equations to describe the kinetic isotope effect during microbial substrate transformation. *Water Resour.* **45**, 937–948.

Wegener, G. 2008 *Methane Oxidation and Carbon Assimilation in Marine Sediments*. Dissertation, Bremen University, p. 153.

First received 19 March 2019; accepted in revised form 5 June 2019. Available online 14 June 2019